UDC 551.510.53

1969
THE QUEEN'S AWARD
TO INDUSTRY

RESEARCH DEPARTMENT

REPORT

M.F. PROPAGATION:
the behaviour of the normal ionosphere during the night and at sunrise

No. 1971/22

Research Department, Engineering Division
THE BRITISH BROADCASTING CORPORATION

RESEARCH DEPARTMENT

M.F. PROPAGATION: THE BEHAVIOUR OF THE NORMAL IONOSPHERE DURING THE NIGHT AND AT SUNRISE

Research Department Report No. **1971/22**

UDC 551.510.53

This Report may not be reproduced in any form without the written permission of the British Broadcasting Corporation

It uses SI units in accordance with B.S. document PD 5686

Work covered by this report was undertaken by the BBC Research Department for the BBC and the ITA

D. Maurice

P. Knight, B.A., M.I.E.E.

Head of Research Department

(RA-81)

Research Department Report No. **1971/22**

M.F. PROPAGATION: THE BEHAVIOUR OF THE NORMAL IONOSPHERE DURING THE NIGHT AND AT SUNRISE

Section	Title	Page
	Summary	1
1.	Introduction	1
2.	Radio waves in the ionosphere	1
3.	Measuring the properties of the ionosphere	1
4.	The collision-frequency profile	2
5.	The critical frequency of the E layer	2
6.	Electron-density profiles	5
	6.1. Night-time profiles	5
	6.2. Sunrise profiles	10
7.	Conclusions	10
8.	References	10
	Appendix 1: The relationship between the critical frequencies of the ordinary and extra-ordinary waves	12
	Appendix 2: Details of measuring sites	13
	Appendix 3: Details of time zones	13

(RA-81)

© BBC 2003. All rights reserved. Except as provided below, no part of this document may be reproduced in any material form (including photocopying or storing it in any medium by electronic means) without the prior written permission of BBC Research & Development except in accordance with the provisions of the (UK) Copyright, Designs and Patents Act 1988.

The BBC grants permission to individuals and organisations to make copies of the entire document (including this copyright notice) for their own internal use. No copies of this document may be published, distributed or made available to third parties whether by paper, electronic or other means without the BBC's prior written permission. Where necessary, third parties should be directed to the relevant page on BBC's website at http://www.bbc.co.uk/rd/pubs/ for a copy of this document.

June 1971

Research Department Report No. 1971/22
UDC 551.510.53

M.F. PROPAGATION: THE BEHAVIOUR OF THE NORMAL IONOSPHERE DURING THE NIGHT AND AT SUNRISE

Summary

This report contains a survey of published electron-density and collision-frequency data for the night-time ionosphere. A set of idealised ionospheric profiles for the night-time and sunrise periods is presented; these are intended for use with a medium-frequency ray-tracing computer program.

1. Introduction

A computer program which traces the paths of waves traversing the ionosphere and calculates their attenuation has been described.[1] Knowledge of the characteristics of the ionosphere is an essential requirement for this program, because both the path of the wave and its attenuation depend on the state of the ionosphere existing at the time.

The computer program is intended for use at medium frequencies (m.f.), although it may be used at higher frequencies if required. At m.f., interest in the ionosphere is confined to the period from just before sunset to an hour after sunrise, because m.f. ionospheric waves are heavily attenuated during the day. At night they may be reflected either from the E layer or from the lower part of the F layer.

The diurnal changes of the ionosphere which are responsible for the propagation of m.f. waves at night depend mainly on the times of sunset and sunrise; the observed seasonal variations are minimised if these times, rather than a fixed hour, are used as references. However the behaviour of the ionosphere varies considerably from night to night and during the course of the solar cycle. It is also disturbed from time to time by aurora, magnetic storms and the occurrence of abnormally intense ionisation (sporadic E).

To simplify the use of the computer program, a set of profiles for the undisturbed or "normal" ionosphere has been derived from published measurements and is presented here. Solar-cycle and sporadic variations are regarded as deviations from the mean condition, and their effects are being studied by statistical methods.[2] The diurnal variation has been taken into account by postulating a set of idealised profiles for specified times relative to sunset or sunrise.

2. Radio Waves in the Ionosphere

During the day, radiation from the sun ionises the upper atmosphere at certain heights, producing positive ions and free electrons. The electrons, being relatively light, are influenced by radio waves and account for the refracting properties of the ionosphere. Collisions between electrons and heavy particles* occur frequently and are responsible for dissipating the energy imparted to the electrons by the radio wave; when collisions occur power is absorbed and the wave is attenuated. The two parameters of the ionosphere which concern radio wave propagation are therefore the electron density and the collision frequency.

The collision frequency depends mainly on atmospheric pressure and decreases approximately exponentially with height above the Earth. The electron density is controlled by radiation from the sun which causes certain constituents of the atmosphere to be ionised, at various heights. Thus the F layer, which is formed at heights above 200 km, is produced by the ionisation of atomic oxygen by X-rays and by short ultra-violet radiation. The E layer, whose maximum electron density occurs at about 110 km, arises from the ionisation of molecular oxygen and nitrogen by the same radiation. The D region, which is really an enhancement of the lower edge of the E layer, is the result of the ionisation of nitric oxide (a minor constituent of the atmosphere) by the intense Lyman-α line of the ultra-violet spectrum.

At sunset the ionising radiation is cut off and the ionisation decreases as a result of recombination between electrons and positive ions. The recombination is most rapid at the lowest heights; thus the D region, which is mainly responsible for the attenuation of radio waves, disappears rapidly, while the F layer decays much more slowly. Shortly before sunrise, ionisation recommences and the various layers rapidly attain their day-time values.

3. Measuring the properties of the ionosphere

Considerable progress has been made in the study of the ionosphere during the last decade and the following techniques are now available for determining electron densities and collision frequencies below the F layer:[3,4]

---

*In the lower ionosphere, collisions with neutral molecules predominate.

(1) Ionospheric sounders,[5] which record photographically the time lapse between the transmission and reception of vertically-incident radio waves as a function of frequency; the recordings are known as *"ionograms"*. This method, which has been in use since 1926, gives a reliable measurement of the maximum electron densities of the E and F layers, and some indication of their shape, but it yields little information about the important D region.

(2) Measurement of the phase and amplitude of v.l.f. and l.f. radio waves.[6,7] An ionospheric model is postulated and is then adjusted until measured and theoretical reflection coefficients agree, the latter being computed by the *full wave-integration* method.[8] Electron densities for the D and lower E region have been derived in this way.

(3) Measurement of *partial reflections* of h.f. radio waves, using a high-power vertical-incidence radar.[9] Electron densities in the lower ionosphere are deduced from the relative amplitudes of ordinary and extraordinary waves, received in advance of the main echoes.

(4) Measurement of *incoherent scatter* (Thomson scatter) of v.h.f. radio waves, using a high-power vertical-incidence radar.[10,11] This method is particularly useful for exploring the night-time "valley" between the E and F layers.

(5) The use of ionospheric *cross-modulation.*[12] Alternate h.f. radio pulses descending after reflection, encounter high-power up-going pulses which modify the ionospheric absorption. Electron densities at the height at which the pulses meet may be deduced from the relative amplitudes of alternate downcoming pulses.

(6) *The use of rockets.* Electron densities and collision frequencies may be measured directly with rocket-borne probes[13] or deduced from radio signals received from rocket-borne transmitters.[14] Rocket measurements reveal the fine detail of the structure of the ionosphere but may not show average conditions.

This report is largely a survey of the results of measurements made at night by the various methods described above. Night-time measurements constitute a relatively small proportion of the total number of measurements which have been made.

4. The collision-frequency profile

In the magneto-ionic theory[15,16] the effect of collisions between electrons and heavy particles is taken into account by adding a friction term to the equation of motion of an electron in an electromagnetic field. This procedure is justified by assuming that free electrons obey the laws of kinetic gas theory and have a Maxwellian velocity distribution. More recent laboratory experiments[17,18] have shown, however, that electron-molecule collisions do not obey these laws; it has been found that the frequency of collisions between electrons and nitrogen molecules (the collisions mainly responsible for the absorption of radio waves) is not proportional to the electron velocity, as would be expected, but to the square of the velocity.[19] The consequence to the magneto-ionic theory has been studied in detail by Sen and Wyller[20] and a simplified treatment has been given by Budden,[21] the conclusion being that the magneto-ionic theory is still valid provided an effective collision frequency is used.

It is customary to express the electron-molecule collision frequency in terms of the collision frequency which would be observed if the electrons shared their total thermal energy equally; this is referred to as the mon-energetic collision frequency ν_m.

It has been shown[20] that the effective collision frequency (ν_{eff}) is equal to $1{\cdot}5\nu_m$ when $\nu_m \gg \omega$ and $2{\cdot}5\nu_m$ when $\nu_m \ll \omega$, where ω is the angular frequency of the wave propagating through the medium. Following Bradley,[22] it is arbitrarily assumed here that the ratio ν_{eff}/ν_m is equal to 1·5 for $\nu_m \geqslant 4\omega$ and 2·5 for $\nu_m \leqslant \omega/4$ with a smooth transition for intermediate values.

The basic physical quantity about which knowledge is sought is ν_m, since ν_{eff} depends on the frequency of the wave. Measurements of temperature and pressure may be used to calculate ν_m directly, or it may be deduced from radio wave measurements of ν_{eff}. Results obtained by the two methods show good agreement below 90 km, but discrepancies are apparent at greater heights, for reasons which are not yet understood. Fig. 1*(a)* shows collision frequency vs height profiles derived from a comprehensive survey[23] of measurements reported by a large number of workers, the continuous curves being deduced from pressure measurements. Also shown are values derived from radio measurements at heights above 80 km; values measured at lower heights agree extremely well with the continuous curves but are too numerous to be distinguished.

The seasonal variations in collision frequency are small in tropical latitudes but increase as polar latitudes are approached.[24] They are thought to be correlated to some extent with corresponding variations of electron density so that the net effect approximates to a small change in the scale height of the ionosphere. Since interest is centered here on the mean ionosphere, these variations will not be considered further. Fig. 1*(b)* shows the collision frequency profile ν_m which is the best fit to the curves and points of Fig. 1*(a)*, together with a curve for ν_{eff} for 1 MHz, calculated from ν_m by the arbitrary rule stated earlier. This curve for ν_{eff} may be used for all frequencies in the m.f. band with little error.

5. The critical frequency of the E layer

The highest frequency which is reflected at vertical incidence by a layer is known as its critical frequency, reflection of the ordinary wave being implied unless

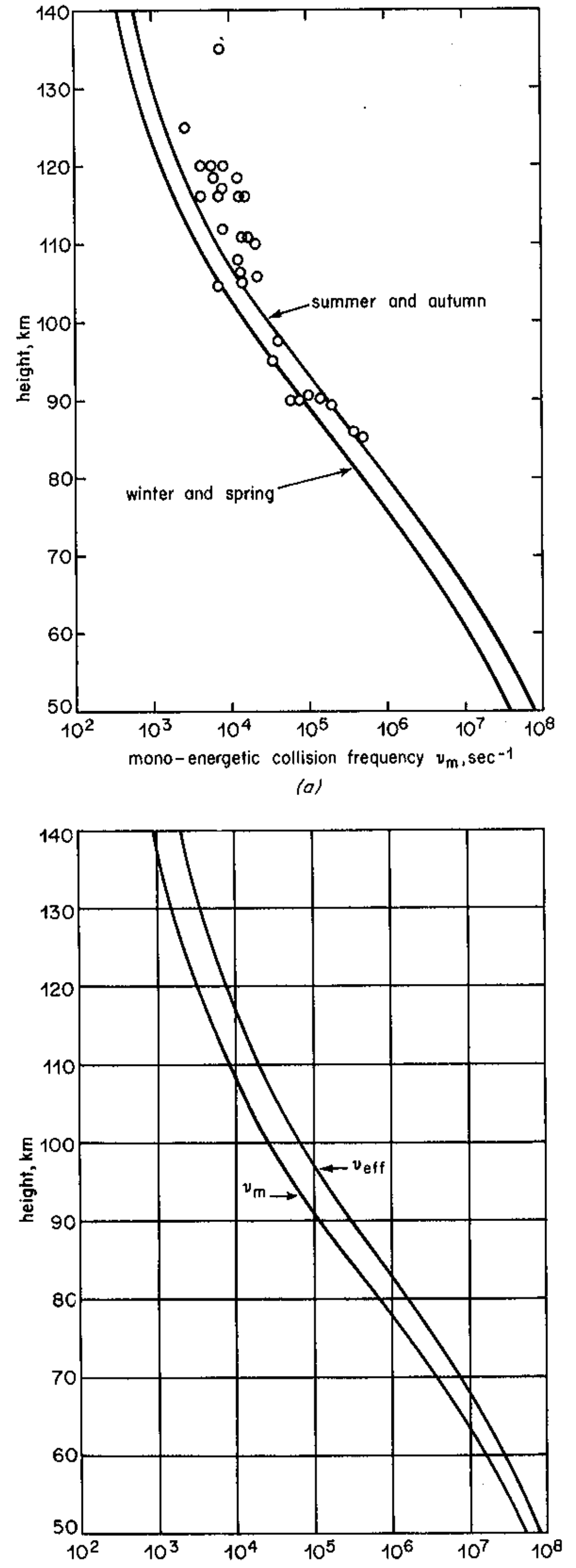

Fig. 1 - Collision frequency

(*a*) Measured values

——— Values deduced from pressure measurements by Thrane and Piggott (Reference 23)

o Values measured above 80 km by radio methods, from Fig. 6 of Reference 23

(*b*) Average values

ν_{eff} is calculated for 1 MHz

otherwise stated. The critical frequency of the ordinary wave depends only on the electron density at the peak of the layer* and is unaffected by the Earth's magnetic field. Measurement of the critical frequency therefore enables the maximum electron density to be determined, the height at which the peak occurs being calculated from the delay time of pulses reflected at slightly lower frequencies.

In the normal E layer the maximum electron density occurs at a height of about 110 km. Thin layers of intense ionisation (sporadic E) may occur over limited areas at heights between 90 and 120 km; these layers are believed to be concentrations of electrons from the normal ionosphere resulting from ionospheric winds. An intermediate layer is sometimes formed at a height of about 150 km at night; it is similar to the normal E layer but slightly more intense and is associated with geomagnetic disturbances.[25] Since this report is concerned with the normal E layer, neither sporadic E layers nor the intermediate layer will be considered further.

The critical frequency of the normal E layer is about 3 MHz during the day and falls to abour 1·5 MHz at sunset. It continues to fall after sunset, reaching a limiting value of about 0·5 MHz late at night. About 2 hours before sunrise it starts to rise, reaching a value of about 1·5 MHz at sunrise.

During the night the critical frequency lies within the m.f. broadcasting band and is difficult to measure because of interference. It may, however, be calculated from the critical frequency of the extraordinary wave,[25] as described in Appendix 1, or deduced from absorption measurements.[26]

E layer critical frequencies measured at Boulder (USA),[25] Slough (UK),[26] Tsumeb (S.W.Africa)[27] and Huancayo (Peru)[25] are compared in Fig. 2*(a)*. All the measurements shown in Fig. 2 are referred to the times at which the upper limb of the sun sets and rises, when seen from sea level; these times may be obtained from published tables.[28] Although the sun sets about 40 minutes later in the E layer its rays are considerably weakened by their passage through the Earth's atmosphere. Consequently there is some justification for adopting ground sunset and sunrise times as references, and they are used throughout this report.

No significant difference is found between critical frequencies measured at sunset and sunrise.[25] Fig. 2*(a)* shows that the critical frequency during the night depends to some extent on the season and on solar activity. The Boulder measurements shown by the full lines include a small proportion of reflections from the intermediate layer and may therefore show median critical frequencies which are slightly greater than the true values for the normal E layer. This was taken into account in drawing the curve shown in Fig. 2*(b)*, which shows how the critical frequency of the normal E layer varies, on average, during the night.

---

*The critical frequency in kHz is equal to $(80{\cdot}61N)^{1/2}$ where N is the electron density in cm^{-3} at the peak of the layer. At this point the critical frequency is equal to the local value of the plasma frequency. The plasma frequency at any point in the ionosphere is the lowest ordinary-wave frequency which is able to propagate when collision effects are small; it is analogous to the cut-off frequency of a waveguide.

TABLE 1

Night-time Electron-density Measurements

Profile Number	Measured at	Type of Measurement	Date	Time	Time after Sunset	Reference
1	Boulder	Ionogram	19. 2. 58	1700 MST	−0·7	39 (Fig. 5*a*)
2	Boulder	Ionogram	20. 4. 60	1800 MST	−0·7	39 (Fig. 4)
3	Malvern	Incoherent scatter	20. 5. 68	1920 UT	−0·7	11 (Fig. 4)
4	Boulder	Ionogram	19. 2. 58	1730 MST	−0·2	39 (Fig. 5*a*)
5	Kagoshima	Rocket	20. 10. 66	1730 JST	−0·2	50 (Fig. 1)
6	Wallops I	Rocket	5. 12. 62	1700 EST	0·3	33 (Fig. 9)
7	Wallops I	Rocket	7. 10. 64	1804 EST	0·5	33 (Fig. 11)
8	Kagoshima	Rocket	18. 3. 65	1907 JST	0·8	34 (Fig. 52)
9	Kagoshima	Rocket	10. 8. 66	2137 JST	1·6	49 (Fig. 3)
10	Malvern	Incoherent scatter	22. 5. 68	2141 UT	1·6	48 (Fig. 3*a*)
11	Boulder	Ionogram	19. 2. 58	1930 MST	1·8	39 (Fig. 5*a*)
12	Hammaguir	Rocket	22. 10. 65	2019 UT	2·2	38 (Fig. 3)
13	Akita	Rocket	26. 9. 60	2025 JST	2·9	25 (Fig. 4*a*)
14	Wallops I	Rocket	17. 8. 61	2206 EST	3·3	33 (Fig. 5)
15 (a)	off Peru Coast	Rocket	26. 3. 65	2200 EST	3·4	45 (Figs. 1*f* and 6*b*)
15 (b)	Huancayo	Ionogram		2215 EST		
16	Churchill	Partial reflection	25. 10. 63	2000 CST	3·5	42 (Fig. 20)
17	Wallops I	Rocket	22. 6. 65	2300 EST	3·5	53 (Fig. 3)
18	Wallops I	Ionogram	3. 2. 66	2100 EST	3·6	41 (Fig. 8)
19	Boulder	Ionogram	20. 4. 60	2230 MST	3·8	39 (Fig. 4)
20	Malvern	Incoherent scatter	21. 5. 68	2359 UT	3·9	Private communication
21	Boulder	Ionogram	19. 2. 58	2200 MST	4·3	39 (Fig. 5*a*)
22	Wallops I	Rocket	7. 4. 66	2301 EST	4·5	35 (Fig. 2)
23	Eglin AFB	Rocket	10. 11. 65	2210 EST	4·6	37 (Fig. 3)
24	Arecibo	Incoherent scatter	11. 8. 67	0003 AST	5·1	54 (Fig. 3)
25	Boulder	Ionogram	21. 4. 60	0000 MST	5·2	39 (Fig. 4)
26	Boulder	Ionogram	19. 2. 58	2330 MST	5·8	39 (Fig. 5*b*)
27	Eglin AFB	Rocket	17. 11. 65	2320 EST	5·8	37 (Fig. 5)
28	Huancayo	Ionogram	18. 3. 65	0000 EST	5·8	45 (Fig. 6*a*)
29	Huancayo	Ionogram	27. 3. 65	0000 EST	5·9	45 (Fig. 6*a*)
30	Malvern	Incoherent scatter	21. 5. 68	0200 UT	5·9	11 (Fig. 4)
31	Churchill	Partial reflection	8. 3. 65	0000 CST	5·9	42 (Fig. 7)
32	Churchill	Partial reflection	9. 3. 65	0000 CST	5·9	42 (Fig. 7)
33	Wallops I	Rocket	12. 4. 63	0530 UT	6·0	31 (Fig. 1)
34	Boulder	Ionogram	20. 2. 58	0000 MST	6·3	39 (Fig. 5*b*)
35	Wallops I	Rocket	22. 2. 68	0009 EST	6·4	53 (Fig. 2)
36	Arecibo	Incoherent scatter	18. 2. 67	0115 AST	6·7	54 (Fig. 4)
37	Boulder	Ionogram	21. 4. 70	0130 MST	6·7	39 (Fig. 4)
38	Boulder	Ionogram	20. 2. 58	0030 MST	6·8	39 (Fig. 5*b*)
39	Pt. Arguello	Ionogram	4. 10. 65	0035 PST	6·9	40 (Fig. 5)
40	Woomera	Rocket	15. 8. 62	0050 LMT	7·2	32 (Fig. 12)
41	Arecibo	Incoherent scatter	17. 1. 67	0135 AST	7·3	54 (Fig. 3)
42	Arecibo	Incoherent scatter	18. 2. 67	0149 AST	7·3	54 (Fig. 4)
43 (a)	off Peru Coast	Rocket	18. 3. 65	0141 EST	7·5	45 (Figs. 1*b* and 6*b*)
43(b)	Huancayo	Ionogram		0115 EST		
44	Arecibo	Incoherent scatter	18. 2. 67	0208 AST	7·6	54 (Fig. 4)
45	Wallops I	Rocket	22. 2. 68	0130 EST	7·7	53 (Fig. 2)
46	Boulder	Ionogram	20. 2. 58	0130 MST	7·8	39 (Fig. 5*b*)

Table 1 cont'd

Profile Number	Measured at	Type of Measurement	Date	Time	Time after Sunset	Reference
47	Boulder	Ionogram	21. 4. 60	0300 MST	8·2	39 (Fig. 4)
48	Boulder	Ionogram	20. 2. 58	0200 MST	8·3	39 (Fig. 5c)
49	Arecibo	Incoherent scatter	18. 2. 67	0246 AST	8·3	54 (Fig. 4)
50	Arecibo	Incoherent scatter	4. 2. 67	0301 AST	8·6	54 (Fig. 3)
51	Arecibo	Incoherent scatter	18. 2. 67	0325 AST	8·9	54 (Fig. 4)
52	Slough	Full-wave integration	Summer and Equinox		9·0	6 (Fig. 7)
53	Slough	Full-wave integration	(Summer and Equinox (Winter		9·0	6 (Fig. 7)
54	Slough	Full-wave integration	Winter		9·0	6 (Fig. 7)
55	Arecibo	Incoherent scatter	18. 2. 67	0345 AST	9·2	54 (Fig. 4)
56	Wallops I	Rocket	22. 2. 68	0300 EST	9·3	53 (Fig. 2)
57	Boulder	Ionogram	20. 2. 58	0300 MST	9·3	39 (Fig. 5c)
58	off Peru Coast	Rocket	22. 3. 65	0349 EST	9·4	36 (Fig. 3)
59	Arecibo	Incoherent	18. 2. 67	0403 AST	9·5	54 (Fig. 4)
60	Wallops I	Rocket	22. 2. 68	0430 EST	10·7	53 (Fig. 2)

Profile No. 8 is not shown in Fig. 3.

Details of measuring sites are given in Appendix 2.

Details of time zones are given in Appendix 3.

References are listed in Section 6.

According to simple theory, the rate at which the electron density decreases during the night is proportional to the square of the number of electrons which remain. The shape of the curve of Fig. 2*(b)* is not, however, consistent with this simple theoretical model. It will be seen that the critical frequency tends towards a constant value late at night, and it is thought that the residual ionisation is caused by ultra violet radiation originating from excited hydrogen atoms in the Earth's outer atmosphere (the geocorona).[29] This may also explain why the critical frequency starts to rise at least an hour before the sun illuminates the layer.

6. Electron-density profiles

Published results of about 100 measurements of the night-time ionosphere have been used to derive a set of idealised electron-density profiles for average conditions. In a previous classification of electron-density profiles,[30] the measurements were grouped according to the actual time of day at which they were made. At night, however, the conditions of the lower ionosphere depends mainly on the time which has elapsed since sunset, and at sunrise it is governed mainly by the solar zenith angle. In the present classification, therefore, electron-density profiles measured during the night have been arranged according to the time after sunset at which the measurements were made, while those measured in the sunrise period have been classified according to solar zenith angle.

6.1 Night-time profiles

Table 1 contains details of published night-time electron-density profiles, arranged according to the time, relative to sunset, at which they were measured. The table covers the period from one hour before sunset to two hours before sunrise. Details of the measuring sites are given in Appendix 2.

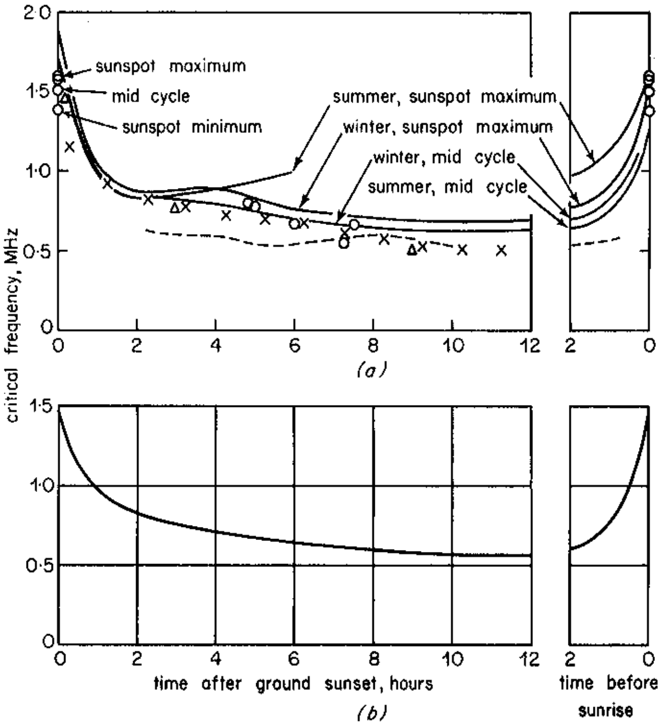

Fig. 2 - Critical frequency of the E layer

(a) Measured values

——— Median values at Boulder for reflections from above 105 km

o Median values at Boulder for reflections from between 105 km and 135 km

x Mean values measured at Tsumeb for heights between 110 and 140 km, at sunspot maximum

Δ Values measured at Slough at sunspot maximum

------ Mean values measured at Huancayo at sunspot minimum

(b) Average values

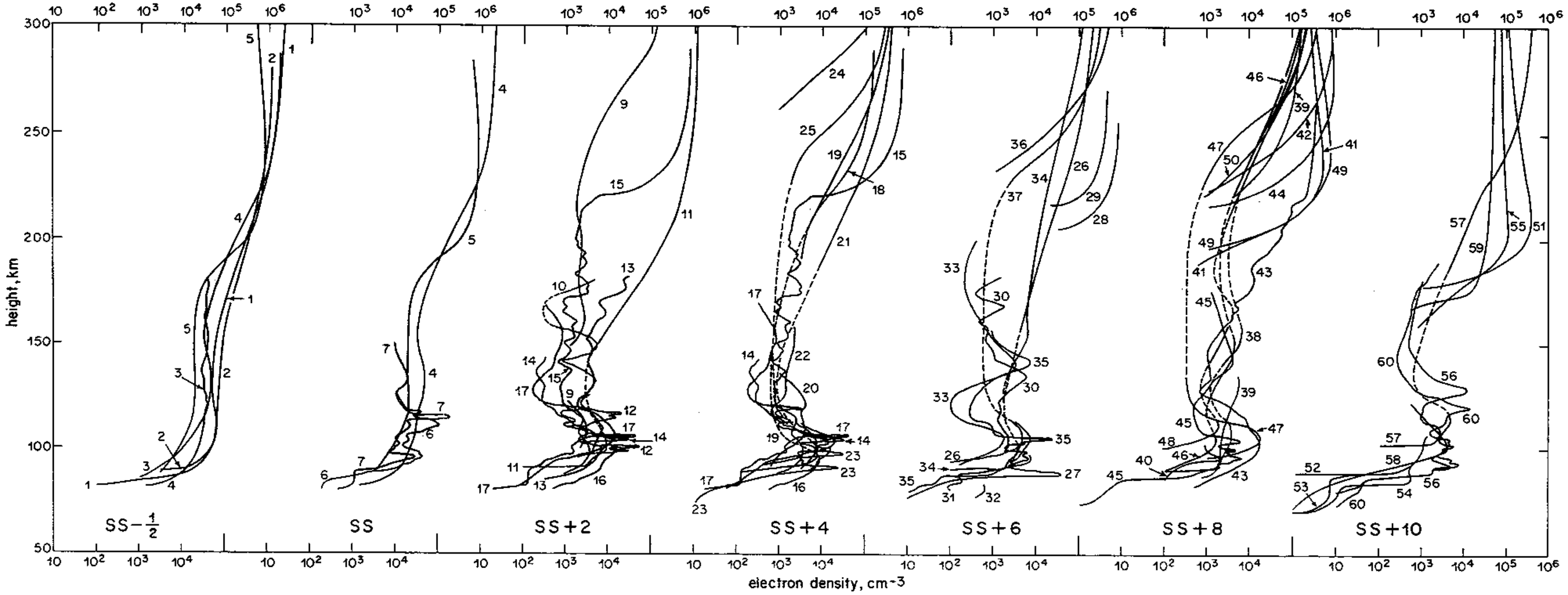

Fig. 3 - Electron-density profiles measured at night

SS + 2, SS + 4 etc. indicate time after sunset in hours

Numbers against curves refer to measurements listed in Table 1

The measurements listed in Table 1 were arranged in groups, to enable measurements made at similar times to be compared. Each group covers a period and is denoted by a nominal time, which is approximately the time at which the E layer critical frequency has the median value for the period. Details of the periods covered by the groups are contained in Table 2.

TABLE 2

Grouping of night-time electron-density profiles

Nominal time	Period covered
SS – 0·5	SS – 0·7 to SS – 0·2
SS	SS – 0·2 to SS + 0·5
SS + 2	SS + 1·6 to SS + 3·5
SS + 4	SS + 3·3 to SS + 5·2
SS + 6	SS + 5·8 to SS + 6·7
SS + 8	SS + 6·8 to SS + 8·6
SS + 10	SS + 8·9 to SS + 10.7

SS = sunset time.
Numbers indicate time after sunset in hours

Fig. 3 shows all the measured profiles grouped in the manner described. The numbers against the curves refer to the serial numbers of the profiles, given in the left-hand column of Table 1. A few profiles appear twice because some of the periods overlap.

Fig. 3 shows a number of sporadic E layers revealed by rocket measurements. Fig. 3 also shows that the normal E layer may vary by a factor of 10 at any particular time. The variation of the F layer is even greater, but this variation is fortunately of no great importance in the present application, since m.f. waves are mainly propagated via the E layer.

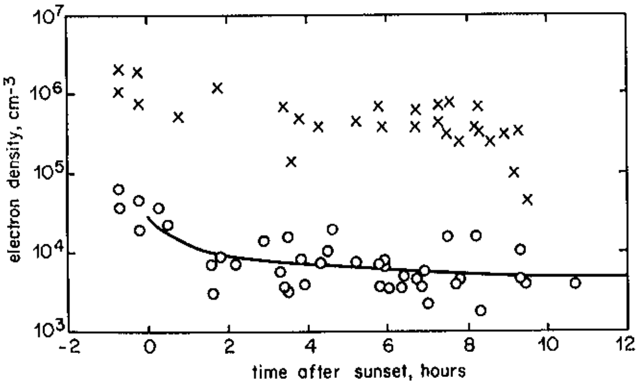

Fig. 4 - Measured maximum electron densities

o Normal E layer × F layer

—— Average curve, calculated from Fig. 2*(b)*

In Fig. 4, the peak electron densities of the normal E and F layers shown in Fig. 3 are plotted against time after sunset. Also shown for comparison is a curve calculated from the average critical frequency curve of Fig. 2*(b)*: the measured electron densities are seen to be reasonably consistent with the average curve.

Fig. 5 shows a set of idealised electron-density profiles for night-time, constructed from the measured profiles.* In drawing these curves the peak electron density of the E layer was adjusted so as to be consistent with critical-frequency measurements. The profile for six hours after sunset may be assumed to apply until two hours before sunrise, since the ionisation of the E layer tends to be maintained to some extent late at night. The onset of daytime conditions first becomes apparent about two hours before sunrise, when the critical frequency of the E layer starts to rise.

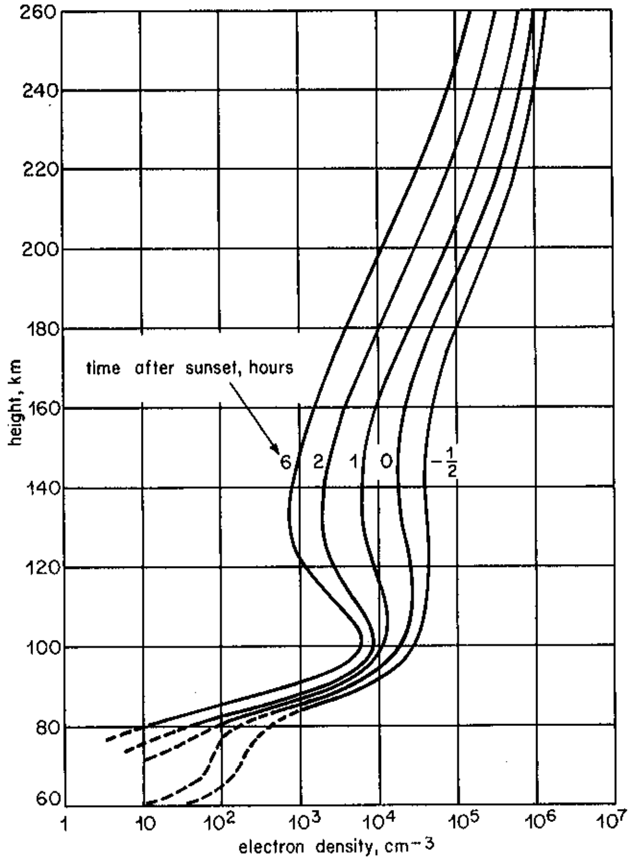

Fig. 5 - Idealised electron-density profiles for night-time

Although the night-time measurements do not contain much information below 80 km the idealised curves have in fact been extended down to 60 km. These extensions are based on detailed measurements of the lower ionosphere made during the sunrise period, which show that the electron density between 60 and 80 km accounts for much of the absorption at sunrise. Now the electron density at these heights is unlikely to be smaller at sunset and it is therefore equally important at this time. For want of better information, the downward extensions of the sunset profiles are based on measurements made at corresponding times at sunrise, described in the next section; they are shown in Fig. 5 as broken lines.

---

* Tabulated values at 1 km height intervals, are contained in Research Department Technical Memorandum No. RA-1078.

TABLE 3

Electron-Density Measurements made during the Sunrise Period

Profile Number	Measured at	Type of Measurement	Date	Time	Solar Zenith Angle	Reference
61	Wallops I	Rocket	27. 10. 61	0435 EST	110°	33 (Fig. 6)
62	Wallops I	Rocket	15. 7. 64	0300 EST	108°	33 (Fig. 10)
63	Boulder	Ionogram	20. 2. 58	0530 MST	105°	39 (Fig. 5*c*)
64	Wallops I	Rocket	7. 11. 62	0525 EST	103°	33 (Fig. 7)
65	Wallops I	Rocket	30. 11. 62	0557 EST	102°	33 (Fig. 8)
66	Arecibo	Incoherent scatter	13. 12. 65	0609 AST	100°	43 (Fig. 2)
67	Slough	Full-wave integration	1948–50		99°	52 (Fig. 2)
68	Wallops I	Rocket	22. 2. 68	0602 EST	99°	53 (Fig. 2)
69	Armidale	Cross-mod.	8. 1. 65		98·1°	44 (Fig. 9)
70	Wallops I	Rocket	8. 10. 64	0523 EST	98°	33 (Fig. 12)
71	Slough	Full-wave integration	1948–50		98°	52 (Fig. 2)
72	Malvern	Incoherent scatter	21. 5. 68	0311 UT	97°	48 (Fig. 3)
73	Armidale	Cross-mod.	8. 1. 65		97·0°	44 (Fig. 9)
74	Slough	Full-wave integration	1948–50		97°	52 (Fig. 2)
75 (a)	Wallops I	Rocket	15. 7. 64	0420 EST	95·8°	24 (Fig. 12) 33 (Fig. 10)
76	Armidale	Cross-mod.	8. 1. 65		95·4°	44 (Fig. 9)
77	Slough	Full-wave integration	1948–50		95°	52 (Fig. 2)
78	Arecibo	Incoherent scatter	13. 12. 65	0630 AST	95°	43 (Fig. 2)
79	Boulder	Ionogram	20. 2. 58	0630 MST	95°	39 (Fig. 5*c*)
80 (a)	Cape Kennedy	Rocket	24. 1. 67		94·9°	51 (Fig. 4)
81	Armidale	Cross-mod.	8. 1. 65		94·3°	44 (Fig. 9)
75 (b)	Wallops I	Rocket	15. 7. 64	0420 EST	94·1°	24 (Fig. 12) 33 (Fig. 10)
82	Armidale	Cross-mod.	8. 1. 65		93·1°	44 (Fig. 9)
80 (b)	Cape Kennedy	Rocket	24. 1. 67		93°	51 (Fig. 4)
83	Slough	Full-wave integration	1948–50		93°	52 (Fig. 2)
84	Slough	Full-wave integration	1948–50		91·5°	52 (Fig. 2)
80 (c)	Cape Kennedy	Rocket	24. 1. 67		91·3°	51 (Fig. 4)
85	Armidale	Cross-mod.	8. 1. 65		91·2°	44 (Fig. 9)
86	Armidale	Cross-mod.	1. 9. 64		90·3°	44 (Fig. 9)
87	Tsumeb	Partial reflection	March 65		90°	46 (Fig. 6)
88	Slough	Full-wave integration	1948–50		90°	52 (Fig. 2)
89	Arecibo	Incoherent scatter	13. 12. 65	0650 AST	90°	43 (Fig. 2)
90	Armidale	Cross-mod.	1. 9. 64		87·9°	44 (Fig. 9)
91	Hammaguir	Rocket	29. 10. 65	0655 UT	87°	38 (Fig. 4)
92	Armidale	Cross-mod.	1. 9. 64		85·1°	44 (Fig. 9)
93	Wallops I	Rocket	15. 7. 64	0525 EST	85°	33 (Fig. 10)
94	Arecibo	Incoherent scatter	13. 12. 65	0712 AST	85°	43 (Fig. 2)
95	Armidale	Cross-mod.	1. 9. 64		82·1°	44 (Fig. 9)
96	Wallops I	Rocket	1. 9. 65	0617 EST	81°	35 (Fig. 2)
97	Arecibo	Incoherent scatter	13. 12. 65	0732 AST	80°	43 (Fig. 2)

Details of measuring sites are given in Appendix 2.

Details of time zones are given in Appendix 3.

References are listed in Section 6.

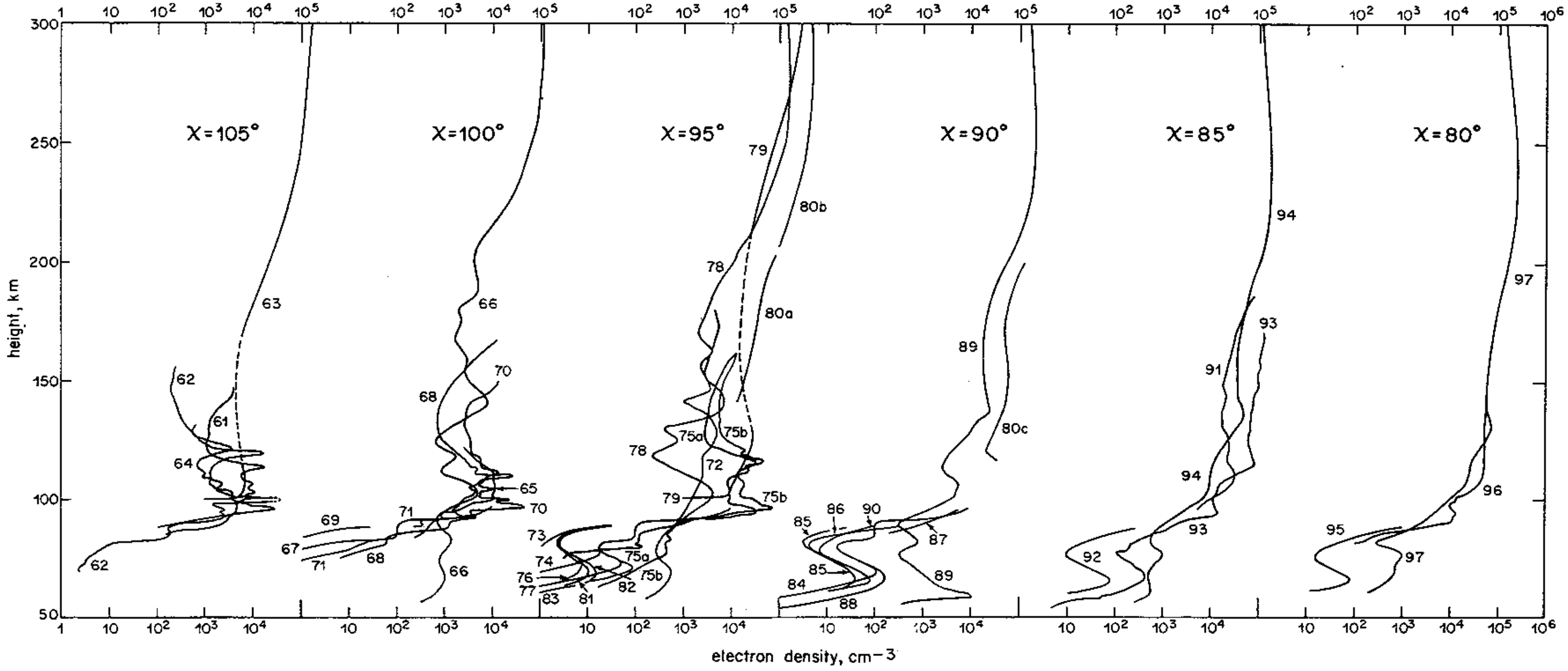

Fig. 6 - Electron-density profiles measured at sunrise

χ = solar zenith angle Numbers against curves refer to measurements listed in Table 3

6.2 Sunrise profiles

During the sunrise period the reionisation process is controlled by the solar zenith angle χ. In temperate and tropical latitudes a 5° change of χ occupies about half an hour.

Table 3 contains details of profiles measured during the sunrise period, arranged according to solar zenith angle. These profiles have also been grouped, measurements made when χ was within $\pm 2{\cdot}5°$ of nominal values at 5° intervals being shown in Fig. 6. The rapid increase in the lower ionosphere, between 60 and 80 km, should be noted. The normal E layer again varies by a factor of 10; there are insufficient measurements to show the variation of the F layer. Fig. 7 shows a set of idealised profiles for the sunrise period constructed from the measurements; the almost constant electron density at about 100 km is an interesting feature.

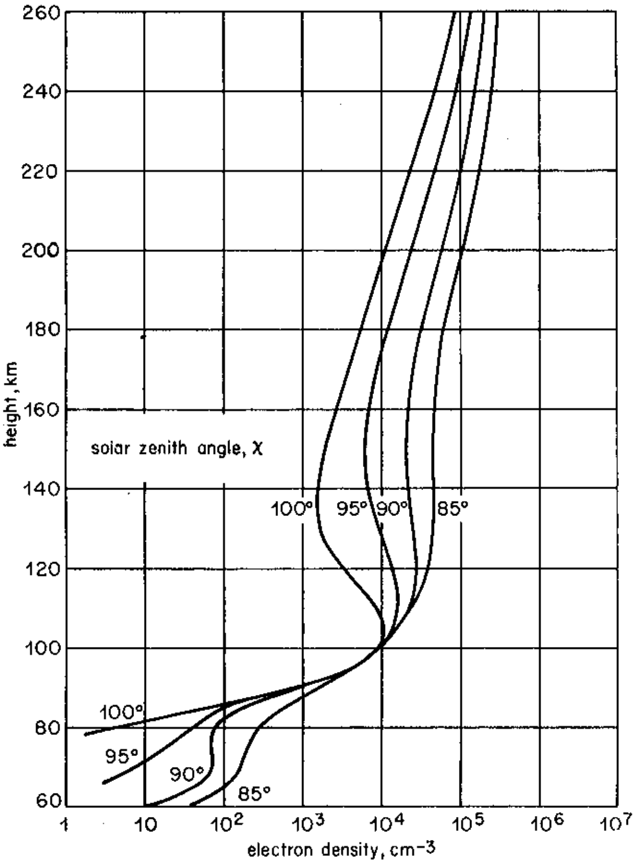

Fig. 7 - Idealised electron-density profiles for the sunrise period

7. Conclusions

The collision-frequency and electron-density profiles presented in this report are based on measurements and are believed to be representative of the average night-time ionosphere. Although day-to-day variations may be large, the average ionosphere varies in a regular manner, the critical frequency of the E layer falling to about 0·5 MHz late at night. The profiles should enable diurnal variations of the average field strength of medium-frequency transmissions to be predicted by ray-tracing methods.

8. References

1. A computer program for calculating sky-wave field strengths at medium frequencies. BBC Research Department Report No. 1970/8. Also in EBU Rev., No. 125-A, pp. 18 – 27, 1971.

2. Variation of medium-frequency sky-wave field strength with solar activity in Europe. BBC Research Department Report No. 1971/11.

3. GORDON, W.E. 1969. Electromagnetic probing of the upper atmosphere. *J. atmos. terr. Phys.*, 1970, **32**, pp. 459 – 466.

4. BOOKER, H.G. *and* SMITH, E.K. 1969. A comparative study of ionospheric measurement techniques. ibid, 1970, **32**, pp. 467 – 497.

5. ECCLES, D. *and* KING, J.W. 1969. Ionospheric probing using vertical incidence sounding techniques. ibid, 1970, **32**, pp. 517 – 538.

6. DEEKS, D.G. 1965. D-region electron distributions in middle latitudes deduced from the reflexion of long radio waves. *Proc. Roy. Soc.*, Series A, 1966, **291**, No. 1426, pp. 413 – 437.

7. CRAIN, C.M. 1969. Ionospheric probing with long wavelength radio waves. *J. atmos. terr. Phys.*, 1970, **32**, pp. 567 – 596.

8. PITTEWAY, M.L.V. 1965. The numerical calculation of wave-fields, reflexion coefficients and polarisations for long radio waves in the lower ionosphere. I. *Phil. Trans. R. Soc.*, Series A, 1965, **257**, 1079, pp. 219 – 241.

9. BELROSE, J.S. 1969. Radio wave probing of the ionosphere by the partial reflection of radio waves, ibid, 1970, **32**, pp. 567 – 596.

10. FARLEY, D.T. 1969. Incoherent scattering at radio frequencies, ibid, 1970, **32**, pp. 693 – 704.

11. HEY, J.S., ROBERTS, J.B.G., TAYLOR, G.N. *and* WATKINS, C.D. 1968. High power radar for ionospheric research. Nature, 1968, **220**, 5170, pp. 865 – 868.

12. FEJER, J.A. 1969. Radio wave probing of the lower ionosphere by cross-modulation techniques. *J. atmos. terr. Phys.*, 1970, **32**, pp. 597 – 607.

13. SAYERS, J. 1969. *In-situ* probes for ionospheric investigations, ibid, 1970, **32**, pp. 663 – 691.

14. MAEDA, K. 1969. Radio propagation effects used on rockets in probing the ionosphere, ibid, 1970, **32**, pp. 647 – 661.

15. APPLETON, E.V. 1932. Wireless studies of the ionosphere. *J. Instn. elect. Engrs.*, 1932, **71**, 430, pp. 642 – 651.

16. RATCLIFFE, J.A. 1959. The magneto-ionic theory and its application to the ionosphere. Cambridge Univ. Press., 1959.

17. HUXLEY, L.G.H. 1959. A discussion of the motion in nitrogen of free electrons with small energies with reference to the ionosphere. *J. atmos. terr. Phys.*, 1959, **16**, 1–2, pp. 46 – 58.

18. PHELPS, A.V. *and* PACK, J.L. 1959. Electron collision frequencies in nitrogen and in the lower ionosphere. *Phys. Rev. Lett.*, 1959, **3**, pp. 340 – 342.

19. DEEKS, D.G. 1966. Generalised full wave theory for energy dependent collision frequencies. *J. atmos. terr. Phys.*, 1966, **28**, pp. 839 – 846.

20. SEN, H.K. *and* WYLLER, A.A. 1960. On the generalization of the Appleton-Hartree magnetoionic formulas. *J. geophys. Res.*, **65**, 12, pp. 3931 – 3950.

21. BUDDEN, K.G. 1964. Effect of electron collisions on the formulas of the magneto-ionic theory. *Radio Sci.*, 1965, **69D**, 2, pp. 191 – 211.

22. BRADLEY, P.A. 1967. Limiting polarization of radio waves of medium and high frequency reflected from the ionosphere. *Proc. Inst. elect. Engrs.*, 1967, **114**, 12, pp. 1837 – 1841.

23. THRANE, E.V. *and* PIGGOTT, W.R. 1966. The collision frequency in the E- and D-regions of the ionosphere. *J. atmos. terr. Phys.*, 1966, **28**, pp. 721 – 737.

24. BELROSE, J.S. *and* BOURNE, I.A. 1966. The electron distribution and collision frequency height profile for the lower part of the ionosphere (the D and lower E regions) – a review of observational data. Proc. conf. on ground-based radio wave propagation studies of the lower ionosphere. Ottawa, Defence Research Board, 1967, Vol. 1, pp. 79 – 96.

25. WAKAI, N. 1966. Mean variations of the night-time ionospheric E layer, ibid, Vol. 2, pp. 552 – 581. Also in *J. Radio Res. Labs. Japan*, 1968, **15**, pp. 109 – 132.

26. PIGGOTT, W.R. 1955. The measurement of normal E-layer critical frequencies at night. *J. atmos. terr. Phys.*, 1955, **7**, pp. 341 – 342.

27. ELLING, W. 1960. Scheinbare Reflexionshöhen und Reflexionsvermögen der Ionosphäre über Tsumeb, Südwest-Africa. *Archiv Elektrischen Ubertragung*, 1961, **15**, 3, pp. 115 – 124.

28. Brown's Nautical Almanac, Glasgow, Brown, Son & Ferguson Ltd., published annually.

29. TOHMATSU, T. *and* WAKAI, N. 1969. An investigation of night-time ionizing sources in low- and mid-latitudes. *Ann. Geophys.*, 1970, **26**, 1, pp. 209 – 211.

30. MAEDA, K. 1969. Mid-latitude electron density profile as revealed by rocket experiments. *J. Geomagn., Geoelect., Kyoto*, 1969, **21**, 2, pp. 557 – 567.

31. CARTWRIGHT, D.G. 1964. A 10-kilocycle per second Doppler observation of the intermediate layer of the night-time ionosphere. *J. geophys. Res.*, 1964, **69**, 19, pp. 4031 – 4035.

32. HALL, J.E. *and* FOOKS, J. 1965. The electron distribution in the quiet D-region derived from rocket measurements of low-frequency propagation. *Planet. Space Sci.*, 1965, **13**, pp. 1013 – 1030.

33. SMITH, L.G. 1965. Rocket observations of sporadic E and related features of the E region. *Radio Sci.*, 1966, **1**, 2, pp. 178 – 186.

34. HIRAO, K. et al. 1966. Direct observations of the ionosphere by sounding rockets during the IQSY. *J. Radio res. Labs. Japan*, 1967, **13**, 66, pp. 75 – 139.

35. HEIKKILA, W.J. et al. 1966. Comparison of ionospheric probe techniques. *Space Research VII*, 1967, pp. 395 – 406.

36. SMIDDY, M. *and* SAGALYN, R.C. 1966. Investigation of electrical phenomena in the equatorial ionosphere, ibid, pp. 428 – 444.

37. SAGALYN, R.C., SMIDDY, M. *and* SULLIVAN, W.P. 1966. Experimental investigation of the night time E region, ibid, pp. 448 – 463.

38. BROSS, P., JACOBS, K.G. *and* RAWER, K. 1966. Direct electron density measurements in the ionosphere below 200 km, ibid, pp. 467 – 476.

39. WAKAI, N. 1967. Quiet and disturbed structure and variations of the night time E region. *J. geophys. Res.*, 1967, **72**, 17, pp. 4507 – 4517.

40. WRIGHT, J.W. 1967. Ionospheric electron-density profiles with continuous gradients and underlying ionization corrections. *Radio Science*, 1967, **2**, 10, pp. 1159 – 1168.

41. LAIRD, A.R. *and* WRIGHT, J.W. 1967. Computation and application of synoptic ionospheric profiles, ibid, pp. 1255 – 1261.

42. BELROSE, J.S., BOURNE, I.A. *and* HEWITT, L.W. 1966. A preliminary investigation of diurnal and seasonal changes in electron distribution over Ottawa, Churchill and Resolute Bay. Proc. conf. on ground-based radio wave propagation studies of the lower ionosphere. Ottawa, Defence Research Board, 1967, Vol. 1, pp. 167 – 188.

43. La LONDE, L.M. 1966. Lower ionosphere echoes observed with incoherent scatter radars, ibid, pp. 229 – 234.

44. SMITH, R.A. et al. 1966. Small perturbation wave interaction in the lower ionosphere: Part 3, measurements of electron densities, ibid, pp. 335 – 358.

45. AIKIN, A.C. *and* BLUMLE, L.J. 1967. Rocket measurements of the E-region electron concentration distribution in the vicinity of the geomagnetic equator. *J. geophys. Res.,* 1968, **73**, 5, pp; 1617 – 1626.

46. THRANE, E.V. et al. 1967. Measurements of D-region electron densities during the International Quiet Sun Years. *J. atmos. terr. Phys,* 1967, **30**, pp. 135 – 150.

47. MECHTLY, E.A. *and* SMITH, L.G. 1967. Growth of the D-region at sunrise, ibid, pp. 363 – 369.

48. TAYLOR, G.N. 1968. Incoherent scatter observations of the E-region. AGARD Conf. Proc., No. 37, 1968.

49. KIMURA, I., NISHINA, R. *and* MAEDA, K. 1967. Rocket observations of the night time ionosphere using the VLF Doppler technique. *Space Research,* 1968, **VIII**, pp. 305 – 312.

50. OYA, H. *and* OBAYASHI, T. 1967. Observation of the microstructure of the ionospheric electron density profile by gyro-plasma probe, ibid, pp. 332 – 338.

51. NAGY, A.F. *and* ROBERTS, W.T. 1967. Diurnal survey of the thermosphere (II). Charged particle results, ibid, pp. 390 – 395.

52. THOMAS, L. *and* HARRISON, M.D. 1969. The electron density distribution in the D-region during the night and pre-sunrise period. *J. atmos. terr. Phys.,* 1970, **32**, pp. 1 – 14.

53. SMITH, L.G. 1969. A sequence of rocket observations of night time sporadic E, ibid, pp. 1247 – 1257,

54. SMITH, D.H. 1969. The comparison of electron density profiles obtained from backscatter observations and ionogram analysis. *Radio Science,* 1970, **5**, 4, pp. 685 – 692.

APPENDIX 1:

The relationship between the critical frequencies of the ordinary and extraordinary waves

At night the critical frequency of the ordinary wave lies within the m.f. broadcasting band and is difficult to measure. It may, however, be deduced from the critical frequency of the extraordinary wave. The relationship between the critical frequencies of the two waves is discussed in this Appendix.

In the magneto-ionic theory the parameters X and Y are defined as follows:

$$X = \left(\frac{f_p}{f}\right)^2$$

$$Y = \frac{f_H}{f}$$

where

f = wave frequency

f_p = plasma frequency, a function of electron density and therefore of height

f_H = gyromagnetic frequency

At vertical incidence the ordinary wave is reflected from the height where $X = 1$ provided collision effects are unimportant, a condition satisfied within the E layer at the frequencies of interest here. At the critical frequency, $X = 1$ at the peak of the layer.

Similarly the extraordinary wave may be reflected at either of the heights where $X = 1 \pm Y$; this result is independent of the direction of the Earth's magnetic field. Below the gyromagnetic frequency the wave can only be reflected at the height where $X = 1 + Y$, since $1 - Y$ is negative. Above the gyromagnetic frequency, reflection at either height is possible, but an upgoing wave encounters the height where $X = 1 - Y$ first and is reflected from this point.

At the extraordinary-wave critical frequency, $X = 1 \pm Y$ at the peak of the layer. From the definitions of X and Y, the critical frequency f_X is given by

$$\left(\frac{f'_p}{f_X}\right)^2 = 1 \pm \frac{f_H}{f_X} \tag{1}$$

where f'_p denotes the value of the f_p at the peak of the layer. Equation (1) represents two quadratic equations in f_X and the pair of equations has two valid solutions* provided f'_p is less than $f_H\sqrt{2}$. This condition is normally satisfied in the E layer at night and the extraordinary wave then has two critical frequencies, which can be shown to differ by f_H.

Since f_p is equal to the ordinary-wave critical frequency f_O, rearrangement of Equation (1) gives the required relationship between f_O and f_X as follows:

$$f_O = f_X(f_X \pm f_H)^{1/2} \qquad (2)$$

Fig. 8 shows this relationship when f_H = 1·25 MHz, a typical value for Europe.

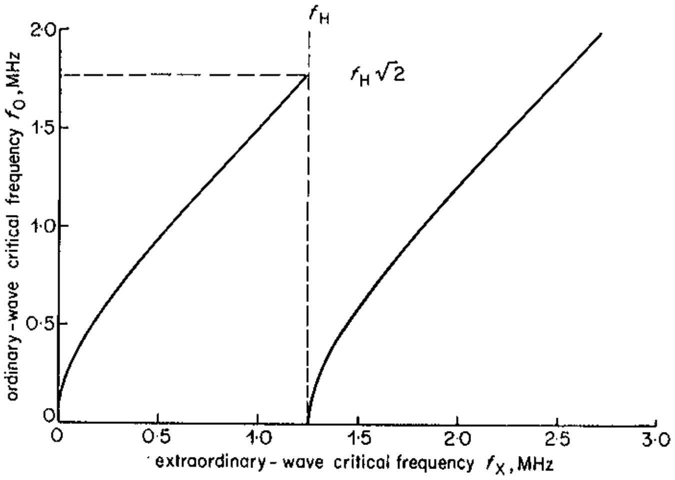

Fig. 8 - Relationship between critical frequencies of ordinary and extraordinary waves
Gyromagnetic frequency f_H, 1·25 MHz

---

*Each equation has a positive solution for all values of f_p, but if $f'_p > f_H\sqrt{2}$, the solution of the equation which applies below the gyromagnetic frequency is greater than f_H and therefore invalid. Thus only one valid solution of the pair of equations exists if $f'_p > f_H\sqrt{2}$.

APPENDIX 2:

List of measuring sites

	Latitude	Longitude	Magnetic Dip Latitude
Akita, Japan	40°N	140°E	55°N
Arecibo, Puerto Rico	18°N	67°W	52°N
Armidale, Australia	30°S	152°E	60°S
Boulder, USA	40°N	105°W	68°N
Cape Kennedy, USA	28°N	80°W	61°N
Churchill, Canada	59°N	94°W	84°N
Eglin AFB, USA	28°N	80°W	62°N
Hammaguir, Algeria	31°N		46°N
Huancayo, Peru	12°S	75°W	2°N
Kagoshima, Japan	31°N	131°E	45°N
Malvern, UK	52°N	2°W	68°N
Pt. Arguello, USA	35°N	120°W	60°N
Slough, UK	52°N	1°W	67°N
Tsumeb, S.W.Africa	20°S	18°E	56°S
Wallops I, USA	38°N	75°W	71°N
Woomera, Australia	31°S	137°E	63°S

APPENDIX 3:

Details of time zones

The abbreviations used in the time columns of Tables 1 and 3 are defined below.

AST	Atlantic Standard Time (GMT – 4 hours)
CST	Central Standard Time (GMT – 6 hours)
EST	Eastern Standard Time (GMT – 5 hours)
JST	Japan Standard Time (GMT + 9 hours)
LMT	Local Mean Time
MST	Mountain Standard Time (GMT – 7 hours)
PST	Pacific Standard Time (GMT – 8 hours)
UT	Universal Time (GMT)